

Scandium effect on undercooling and dendrite morphology of Al-4.5wt% Cu droplets

J. Valloton^{1,*}, A.-A. Bogno¹, H. Henein¹, D.M. Herlach² and D. Sediako³

¹ Advanced Materials and Processing Laboratory, University of Alberta, Edmonton, Canada, T6G 1H9

² Institut für Materialphysik im Weltraum, Deutsches Zentrum für Luft- und Raumfahrt, Cologne, Germany, 51170

³ UBC Okanagan, Kelowna, BC, Canada, V1V 1V7.

* Corresponding author: valloton@ualberta.ca

Abstract

This paper reports on the undercooling and growth morphology of Al-4.5wt%Cu and Al-4.5wt%Cu-0.4wt%Sc with a focus on the effect of Sc addition. It is found that the addition of Sc reduces the undercoolings of both primary phase and eutectic. In addition, the morphology of the Al-4.5wt%Cu-0.4wt%Sc dendrites is less favored in the $\langle 111 \rangle$ direction at similar undercoolings as with Al-4.5wt%Cu. The development of Solidification Continuous Cooling Transformation diagrams that relate the solidification paths to the inherent solidification microstructures is also introduced. The Solidification Continuous Cooling Transformation diagrams are obtained, based on the measurement of phase fractions of a solidified microstructure. The quantitative data is combined with well-established solidification models and phase diagrams to yield undercooling temperatures of individual phases. The thermal history and undercooling of different phases in the solidified alloy are estimated for a wide range of cooling rates (from 10^{-2} K/s to 10^4 K/s). It is found that a minimum cooling rate of about 1 K/s is required to avoid the nucleation of the detrimental intermetallic, W phase in hypo-eutectic Al-Cu-Sc.

30

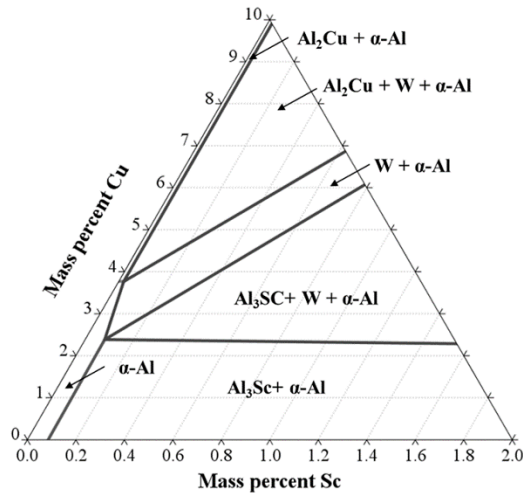
31 **Introduction**

32 Aluminum is the 3rd most abundant element on the planet, accounting for about eight percent of
33 the Earth's crust. Aluminum alloys occupy an important place in various industrial applications,
34 such as automotive and aerospace. This is due to their good mechanical properties coupled with
35 low density (i.e. excellent strength-to-weight ratio), corrosion resistance and castability [1].
36 Aluminum alloys are typically strengthened via precipitation of secondary intermetallic phases
37 from alloying elements in solid solution. Copper is one of the most widely used alloying element
38 due to its well-known age hardening effect characterized by precipitation of finely dispersed
39 Guinier–Preston (GP) zones, θ' and followed by the stable θ phase through heat treatment [2].

40 Lately, the development of commercial age-hardenable aluminum alloys with improved
41 performances has focused on systems forming Al_3X precipitates, such as Al-Sc, Al-Zr or Al-V [3].
42 Of these, Al-Sc alloys have garnered the most attention [4][5]. Age hardening leads to the
43 formation of a dense and homogeneous dispersion of approximately spherical Al_3Sc particles.
44 These nanosized precipitates effectively block the movement of dislocations and grain boundaries
45 and thus stabilize fine-grained structures [5][6][7]. Besides precipitation hardening, addition of Sc
46 to Al-alloys can also act as a grain refiner during casting using hypereutectic additions of Sc.
47 Indeed, Al_3Sc has an FCC structure and a lattice parameter close to that of α -Al [8]. For
48 hypereutectic compositions of Sc, Al_3Sc precipitates will thus act as nuclei for the formation of the
49 aluminum phase [9].

50 Ternary Al-Cu-Sc alloys have been scarcely studied. In addition to the traditional Al_2Cu and Al_3Sc
51 intermetallics, Kharakterova reported one ternary compound, $Al_{8-x}Cu_{4+x}Sc$ ($0 \leq x \leq 2.6$), that can be
52 in equilibrium with α -Al [10][11]. This phase, dubbed W-phase, is found in the Al-rich corner of the
53 Al–Cu–Sc phase diagram, as shown in Figure 1. Recently, Bo et al. carried out a thermodynamic
54 analysis of this system [12]. A good agreement was found between calculated phase equilibria
55 and the reported experimental data from Kharakterova. The W-phase was further evidenced in
56 the work of Bogno et al during solidification of Al-4.5wt%Cu-0.4wt%Sc at low cooling rates [7].
57 Their work showed that the addition of 0.4wt%Sc to Al-4.5wt%Cu did not demonstrate any
58 significant benefit since most of the Sc precipitated as the W-phase. Only a slight hardness
59 increase was observed after heat treatment, which was attributed to the precipitation of the
60 remaining Sc in solid solution within the matrix to form Al_3Sc . In general, the formation of the W-
61 phase is detrimental as it consumes part of the Sc and Cu atoms in the Al matrix. As a

62 consequence, both the precipitation of Al_3Sc and the occurrence of Cu strengthening phases are
63 reduced and this minimizes the positive effect of Sc on the mechanical properties of the alloy [13].



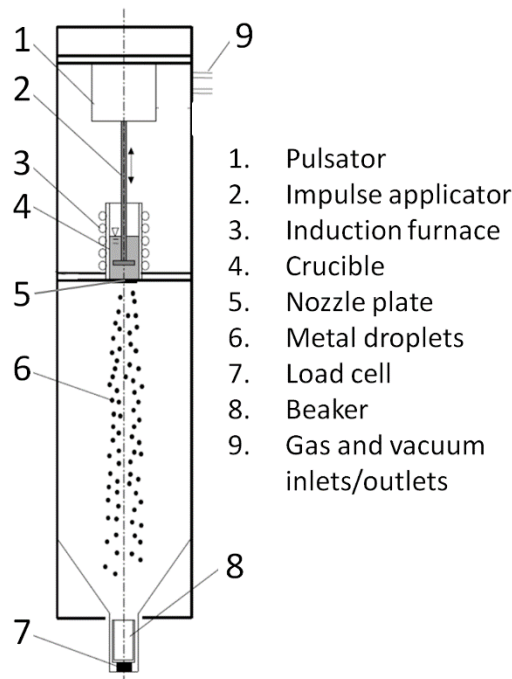
64
65 **Figure 1:** Isothermal section of the Al-rich corner of the Al-Cu-Sc system at 500°C computed
66 with ThermoCalc using the ALDEMO database [14].

67
68 Our previous study of rapidly solidified Al-4.5wt%Cu and Al-4.5wt%Cu-0.4wt%Sc samples
69 showed that with hypoeutectic additions of Sc in Al-4.5wt% Cu, no grain refining effect is observed
70 [15]. Furthermore, rapid solidification supersaturates copper and scandium in the aluminum matrix
71 and in the interdendritic regions, and thus prevents the formation of the W-phase. A dramatic
72 improvement in mechanical properties is observed when Al-4.5wt%Cu-0.4wt%Sc samples are
73 aged, with the microhardness increasing from about 75 HV as-atomized to 120 HV after heat
74 treatment. This is attributed to the precipitation of nanosized Al_3Sc and Al_2Cu particles. Thus, by
75 rapidly solidifying Al-4.5wt%Cu-0.4wt%Sc, the solutionizing and quenching step can be omitted
76 from the regular heat treatment process.

77 As scandium remains a very expensive alloying element, keeping its level low is economically
78 warranted. This work thus reports on the solidification of Al-4.5wt%Cu containing 0, 0.2 and
79 0.4wt%Sc under cooling rates varying from 10^0 K/s to 10^4 K/s by Differential Scanning Calorimetry
80 (DSC), Electro-Magnetic Levitation (EML) and Impulse Atomization (IA). This paper focuses on
81 the effect of Sc on the undercooling and the morphology of the solidified samples and introduces
82 Solidification Continuous Cooling Transformation (SCCT) diagrams for Al-4.5wt%Cu and Al-
83 4.5wt%Cu-0.4wt%Sc.

84 **Experimental methods**

85 Impulse atomization (IA) is a drop tube-type containerless solidification technique where
86 solidifying droplets experience high cooling rates and nucleation undercoolings [16]. It consists in
87 the transformation of a bulk liquid into a spray of liquid droplets that solidify rapidly during free fall
88 by losing heat to a surrounding gas of choice (usually N₂, Ar or He). The base material is melted
89 using an induction furnace and the atomization is achieved by the application of a mechanical
90 pressure (impulse) to the melt in order to push it through a nozzle plate with one or several orifices
91 of known size and geometry. A liquid ligament emanates from each orifice, which in turn breaks
92 up into droplets due to Rayleigh-type instabilities. The solidified powders are then collected in a
93 beaker at the bottom of the tower. IA generates a range of droplets sizes per run, giving a range
94 of cooling rates and undercoolings. The cooling rate is a function of both the droplet size and the
95 gas in the atomization tower and can reach up to ~10⁵ K/s. However, no direct measurement of
96 temperature has been feasible to date. The cooling rates of individual droplets are estimated using
97 a solidification model for atomization developed by Wiskel et al [17][18] while primary and
98 secondary phase nucleation undercoolings are determined using a new, novel methodology
99 described in details in [19], with a summary given below.



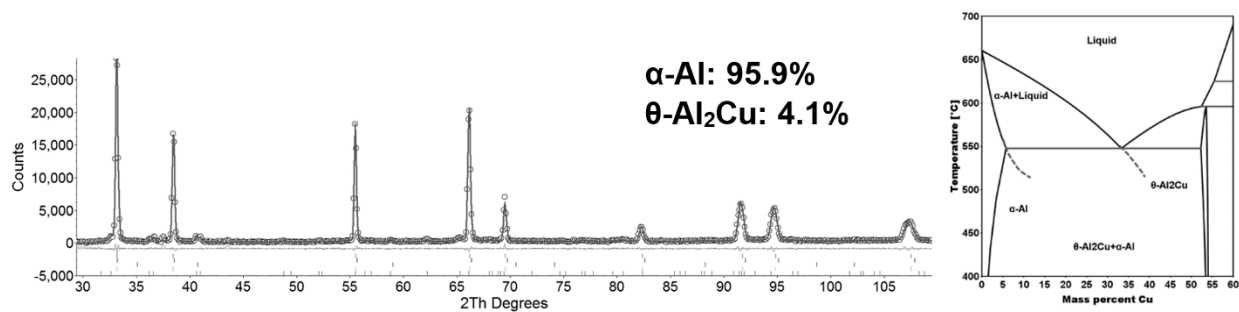
100

101

Figure 2: Schematic view of an impulse atomization apparatus.

102

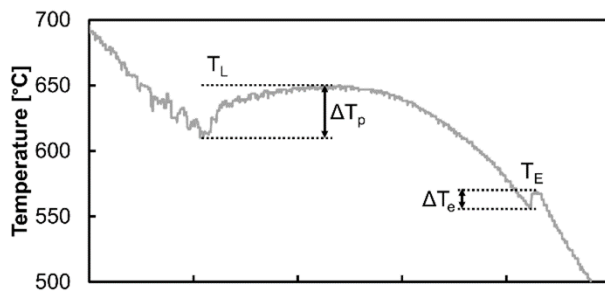
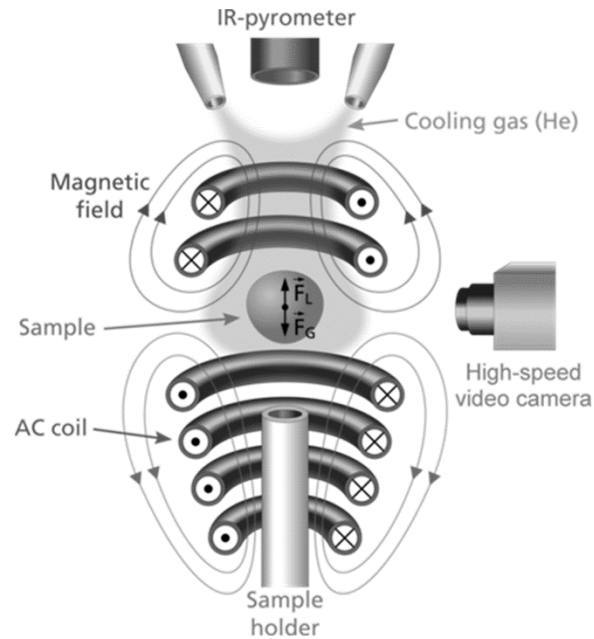
103 The methodology is based on experimental determination of phase fraction using Neutron
104 Diffraction. The eutectic fraction is determined from the fraction of Al_2Cu obtained by Rietveld
105 refinement of the diffraction spectra for an Al-Cu alloy (Figure 3 left). The corresponding eutectic
106 nucleation undercooling is then evaluated from the metastable extension of the solidus and
107 liquidus of the phase diagram of the alloy (Figure 3 right). The primary dendritic nucleation
108 undercooling is subsequently determined using semi-empirical coarsening models of secondary
109 dendrite arms. In the case of Al-4.5wt%Cu-0.4wt%Sc, the same methodology was used with a
110 pseudo-binary phase diagram generated with ThermoCalc.



111
112 **Figure 3:** Left: Neutron diffraction diagram of IA droplets of Al-4.5wt% Cu. The phase fractions
113 are obtained by Rietveld refinement analysis of the diffraction pattern [20]. Right: Al-richer corners
114 of Al-Cu binary phase diagrams. The dashed lines represent the extensions of the solidus and
115 liquidus lines obtained with ThermoCalc using the TTAL7 database.

116
117 Electromagnetic levitation (EML) is a powerful containerless solidification technique for the
118 processing of metallic and semiconductor samples with a large range of undercoolings. A
119 schematic view of the apparatus is shown in Figure 4. An alternating current flowing through a
120 water-cooled levitation coil produces an alternating electromagnetic field. A conducting sample
121 placed within this field is levitated by the Lorentz force F_L which compensates for the gravitational
122 force F_G . Simultaneously, the eddy currents induced in the sample heat and melt the sample by
123 ohmic losses. To solidify the sample, cooling jets of inert gas are used. The temperature of the
124 sample is monitored continuously with a two-color pyrometer (Impac IGA10-LO) with an accuracy
125 of ± 5 K. As shown in Figure 4, this allows for a direct measurement of undercoolings, as well as
126 cooling rates. Detailed information on the EML technique can be found in [21].

127

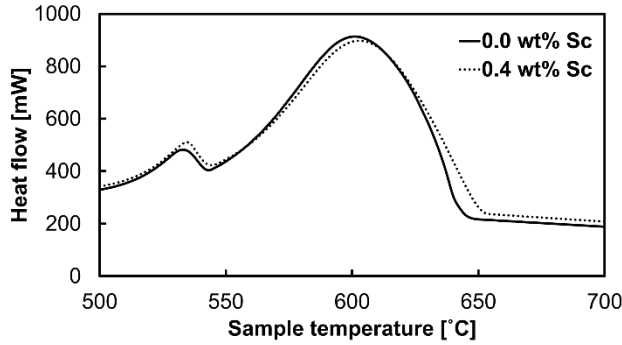


128

129 **Figure 4:** Schematic view of an EML apparatus and typical temperature-time profile obtained
 130 during EML solidification of an Al-4.5wt%Cu sample. Primary and eutectic solidification are clearly
 131 identified by the corresponding recalescence events of undercoolings $\Delta T_p = 34$ K and $\Delta T_e = 13$ K
 132 respectively.

133

134 DSC is a thermal analysis technique used to determine the amount of energy absorbed or
 135 released by a sample as it is heated or cooled in a controlled manner inside a crucible. As a non-
 136 containerless solidification technique, it yields low nucleation undercooling and its cooling rate
 137 (measurable) is limited to a narrow range (50 K/s maximum). In this work Al-Cu and Al-Cu-Sc
 138 alloys were solidified under low cooling rates and low undercooling conditions in a Setaram
 139 Labsys Evo 1600 DSC using alumina crucibles. A typical solidification curve using DSC is
 140 presented in Figure 5. The primary and eutectic nucleation temperatures can be inferred from the
 141 onset of the exothermic peaks.



142

143 **Figure 5:** DSC solidification curves of Al-4.5 wt%Cu and Al-4.5wt%Cu-0.4wt%Sc cooled at 0.8
 144 K/s [7].

145

146 For metallographic analysis, DSC, EML and IA samples were first mounted in epoxy resin.
 147 Grinding was carried out using silicon carbide papers up to grit 1000 (P2500), followed by
 148 mechanical polishing with 3 and 1 μm diamond particles on soft cloths. Final polishing was
 149 performed with a 0.05 μm colloidal silica. Microstructural characterization was carried out using
 150 scanning electron microscopy (SEM) with a Zeiss Sigma FE-SEM running at 20 kV. Cell spacing
 151 measurements were obtained using the line intercept method on selected SEM micrographs
 152 according to ASTM E112-13.

153 Neutron diffraction measurements on IA samples were performed on the C2 neutron
 154 diffractometer located at the Canadian Neutron Beam Centre in Chalk River, Canada.
 155 Measurements were performed using a wavelength of 1.33 \AA from a Si531 monochromator at
 156 $92.7^\circ 2\theta$.

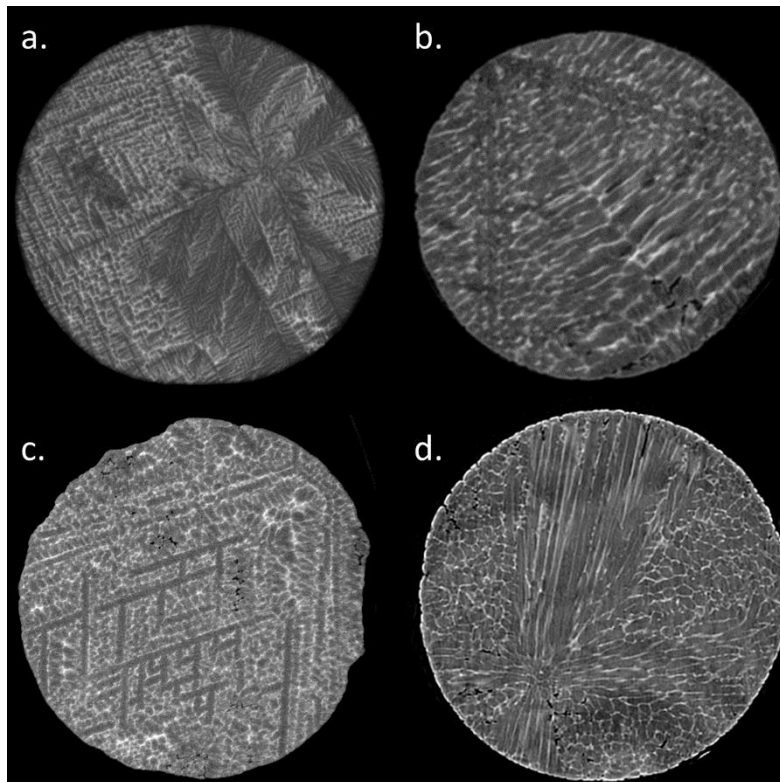
157 Synchrotron X-ray micro-tomography was carried out post-mortem at ESRF (European
 158 Synchrotron Radiation Facility, Grenoble, France) on the ID19 beamline. Two pixel resolutions
 159 were used: a high resolution of 0.18 $\mu\text{m}/\text{voxel}$ (field of view of 369 μm side cube) to analyze in
 160 detail the fine microstructure of small droplets, and a medium resolution of 0.56 $\mu\text{m}/\text{voxel}$ (field of
 161 view of 1146 μm side cube) to scan several small droplets at the same time to derive statistical
 162 data.

163

164 **Results and discussion**

165 Cubic type crystals of metallic alloys such as Al-Cu, Al-Fe and Al-Ni generally grow along $\langle 100 \rangle$
 166 directions due to the anisotropy of the solid-liquid interfacial energy. Under certain conditions (e.g.
 167 high undercooling) dendrites growth deviates from $\langle 100 \rangle$ and unusual and complex morphologies
 168 can develop. For example, in Al-0.6wt%Fe and Al-1.9wt%Fe impulse atomized droplets, a change

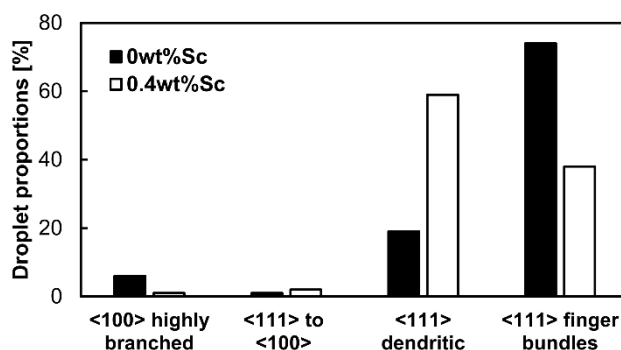
169 in dendrite growth direction from $\langle 100 \rangle$ to $\langle 111 \rangle$ was observed [22]. For IA Al-4.5wt%Cu droplets,
170 an earlier in-depth investigation by Bedel et al [23] revealed four distinct dendritic morphologies
171 using X-Ray microtomography (Figure 6). The highly branched morphology (a) shows dendrite
172 growing along the usual $\langle 100 \rangle$ while microstructural features indicate that dendrite arms develop
173 mostly along $\langle 111 \rangle$ directions in the other three morphologies (b-d). The transition from $\langle 100 \rangle$ to
174 $\langle 111 \rangle$ is attributed to an increase in the solidification growth velocity. At the slowest solidification
175 growth velocity, $\langle 100 \rangle$ arms develop (a). At higher cooling rates and/or undercooling, primary
176 arms start growing along $\langle 111 \rangle$ but higher level arms forming after recalescence are slower and
177 thus grow along $\langle 100 \rangle$ (b). At even higher solidification rates, the droplet solidifies completely
178 with a $\langle 111 \rangle$ growth direction, as illustrated in (c). Finally, at the highest speed, a competition
179 between different $\langle 111 \rangle$ arms originating from the same nucleation point leads to the formation
180 of so-called finger bundles (d). Our collaborative work also showed that as the cooling rate
181 increases, $\langle 111 \rangle$ dendrites are favored and the number of droplets with a finger bundle
182 morphology increases.



183

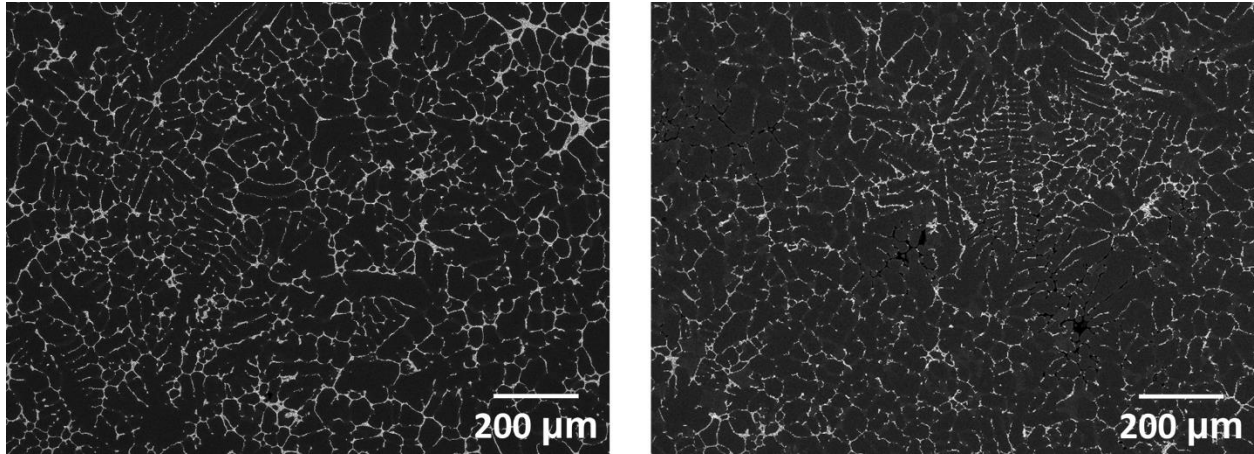
184 **Figure 6:** Typical dendrite morphologies observed in Al-4.5wt%Cu droplets solidified in IA: (a)
185 $\langle 100 \rangle$ highly branched dendrites; (b) $\langle 111 \rangle$ to $\langle 100 \rangle$ dendrite transition; (c) $\langle 111 \rangle$ dendritic
186 morphology; (d) $\langle 111 \rangle$ finger bundle morphology.

187 Figure 7 shows the statistical distribution of the four dendrite morphologies observed in IA droplets
 188 of composition Al-4.5wt%Cu and Al-4.5wt%Cu-0.4wt%Sc solidified in argon with diameters in the
 189 range of 0 to 212 μm . A total of 69 droplets were analyzed for Al-4.5wt%Cu and 91 for Al-
 190 4.5wt%Cu-0.4wt%Sc. When Sc is added, it is observed that the number of droplets with finger
 191 bundles decreases in favor of lower speed morphologies. As the processing gas and the droplet
 192 size range are the same in both cases, the droplet cooling rates are expected to be similar,
 193 regardless of the presence of scandium. Thus, this shift in morphology is attributed to a change
 194 in the droplet undercoolings induced by the addition of Sc, as will be discussed later.



195
 196 **Figure 7:** Statistical distribution of the four morphologies in Al-4.5wt%Cu and Al-4.5wt%Cu-
 197 0.4wt%Sc droplets Impulse Atomized in Ar with a diameter range $0 < d < 212 \mu\text{m}$.

198
 199 Figure 8 shows a representative solidification microstructure of an Al-4.5wt%Cu sample solidified
 200 in EML with a solidification cooling rate of $\sim 9 \text{ K/s}$ and primary and eutectic undercoolings of ΔT_p
 201 $= 34 \text{ K}$ and $\Delta T_e = 13 \text{ K}$, respectively, as well as an Al-4.5wt%Cu-0.4wt%Sc sample solidified at
 202 $\sim 12 \text{ K/s}$ with $\Delta T_p = 6 \text{ K}$ and $\Delta T_e = 4 \text{ K}$. EML samples typically show a cellular microstructure with
 203 no obvious growth direction. Some dendritic remnants can be observed in Figure 8 and in other
 204 EML samples. When present, these dendrites exhibit <100> growth direction in all cases. This
 205 suggests that the growth velocity in EML samples is slower than in IA. This is supported by the
 206 scale of the microstructure, which is one order of magnitude coarser in EML than in IA samples.
 207 Finally, it is observed that the addition of scandium does not alter the morphology of the solidified
 208 EML samples.

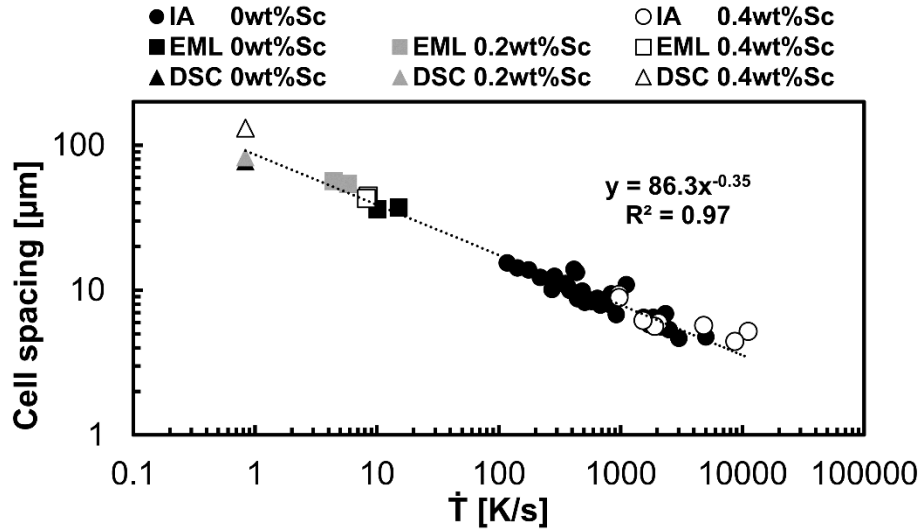


209

210 **Figure 8:** Representative solidification microstructure of Al-4.5wt%Cu solidified in EML at ~9 K/s
 211 with $\Delta T_p = 34$ K and $\Delta T_e = 13$ K (left) and Al-4.5wt%Cu-0.4wt%Sc solidified in EML at ~12 K/s
 212 with $\Delta T_p = 6$ K and $\Delta T_e = 4$ K (right). In both cases, the structure is mostly cellular with some
 213 dendrite remnants showing $\langle 100 \rangle$ growth directions.

214

215 Figure 9 shows the cell spacing measured with the line intercept methods as a function of cooling
 216 rate for DSC, EML and IA samples [15]. Regardless of the solidification technique, the effect of
 217 Sc addition on the microstructures scale is found to be negligible. However, microstructure
 218 refinement is shown to be very dependent on the cooling rate. This relationship follows a power
 219 law of the type $\lambda_2 = A\dot{T}^{-n}$, where λ_2 is the cell spacing, \dot{T} the cooling rate and A and n are constants,
 220 as described by Eskin et al [24]. The values of A and n found in this study are in the range of
 221 values published by Mullis and co-workers in the estimation of cooling rates during close-coupled
 222 gas atomization of Al-4wt%Cu using secondary dendrite arm spacing measurements [25].
 223 Furthermore, the exponent value being very close to the theoretical value of 1/3 [26], the decrease
 224 in cell spacing observed with increasing cooling rate indicates that the final scale of the
 225 microstructure is governed mainly by coarsening.



226

227 **Figure 9:** Variation of cell spacing with cooling rate for Al-4.5 wt% Cu with different Sc levels.

228

229 As EML experiments allow the direct measurement of the temperature profile during solidification,
 230 it is easy to assess the effect of scandium addition on the nucleation behavior of the alloy studied.
 231 Table 1 compiles the average of the measured undercoolings obtained during EML solidification
 232 of Al-4.5wt%Cu samples with the addition of 0, 0.2 and 0.4wt%Sc (9, 7 and 12 solidified samples
 233 respectively). Nucleation being a stochastic event, a range of undercoolings is obtained for each
 234 composition, which is reflected in the standard deviation for each composition in Table 1. It is
 235 clear that the addition of Sc promotes the nucleation of the α -Al and θ -Al₂Cu phases as both the
 236 primary and eutectic undercoolings decrease when Sc is added to the alloy. The primary
 237 undercooling decreases significantly only with a 0.4wt%Sc addition, while both 0.2 and 0.4wt%Sc
 238 exhibit the same change in eutectic undercooling. This suggests that the presence of scandium
 239 in the melt is sufficient to alter the interfacial energy between the Sc containing liquid and Al₂Cu
 240 and to promote nucleation of the intermetallic phase. The results of cooling rate of the liquid
 241 samples, as well as the primary and eutectic undercoolings for each method used is presented in
 242 Figure 10. The same trend is observed, regardless of the cooling rate or solidification technique.

243

244

245

246

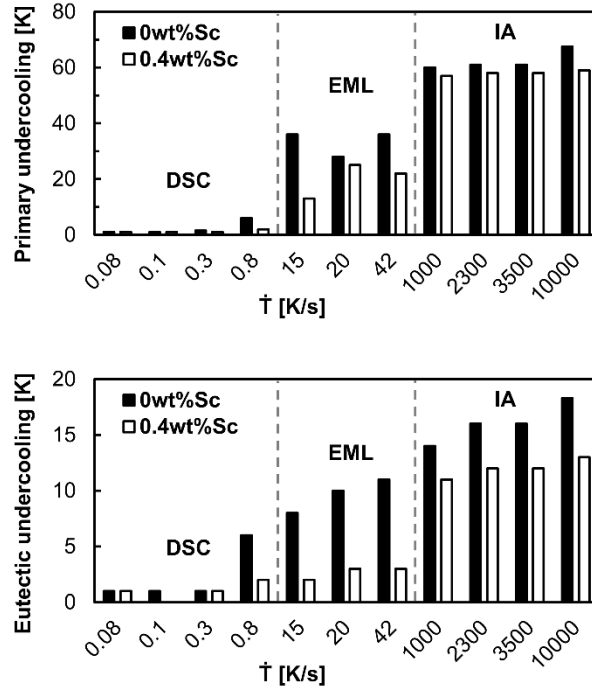
247

248 **Table 1:** Average primary and eutectic nucleation undercoolings during EML solidification.

	ΔT_p [K]	ΔT_e [K]
0 wt% Sc	35.7 ± 6.5	10.1 ± 1.9
0.2 wt% Sc	30.9 ± 6.4	3.6 ± 0.9
0.4 wt% Sc	13.8 ± 5.7	3.7 ± 1.8

249

250



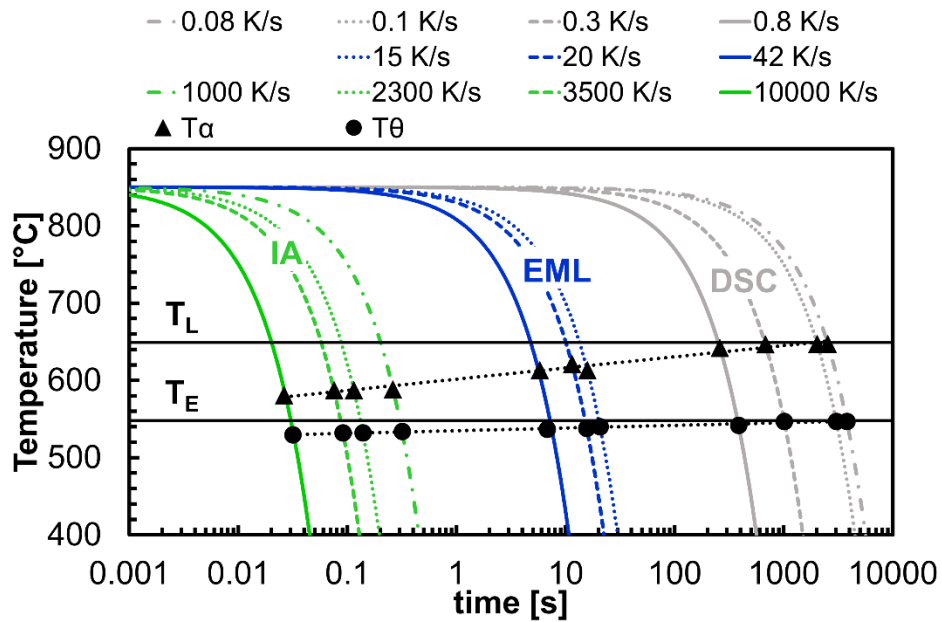
251

252 **Figure 10:** Variation of nucleation undercooling with solidification cooling rate for Al-4.5wt%Cu
 253 and Al-4.5wt%-0.4wt%Sc

254 As reported in a previous contribution, X-ray and Neutron Diffraction of EML and IA samples did
 255 not show the presence of the W-phase. Only in the DSC solidified samples was the W phase
 256 observed [7]. Knowing this, and with the results presented above, the quantification of the
 257 solidification path of Al-4.5wt%Cu and Al-4.5wt%Cu-0.4wt%Sc alloys is possible. In order to
 258 represent the resultant microstructure and relate it to macro-solidification conditions, solidification
 259 continuous cooling transformation (SCCT) curves were developed. To construct these maps, the
 260 liquid cooling rates of the samples were used (imposed for DSC, measured on the temperature-
 261 time profile for EML, and estimated with the atomization model for IA) and the corresponding
 262 undercoolings from Figure 10 were plotted on a CCT diagram (Figure 11 and 12). Also plotted on
 263 these diagrams are the equilibrium liquidus, T_L , and eutectic, T_E , of the respective alloys. From

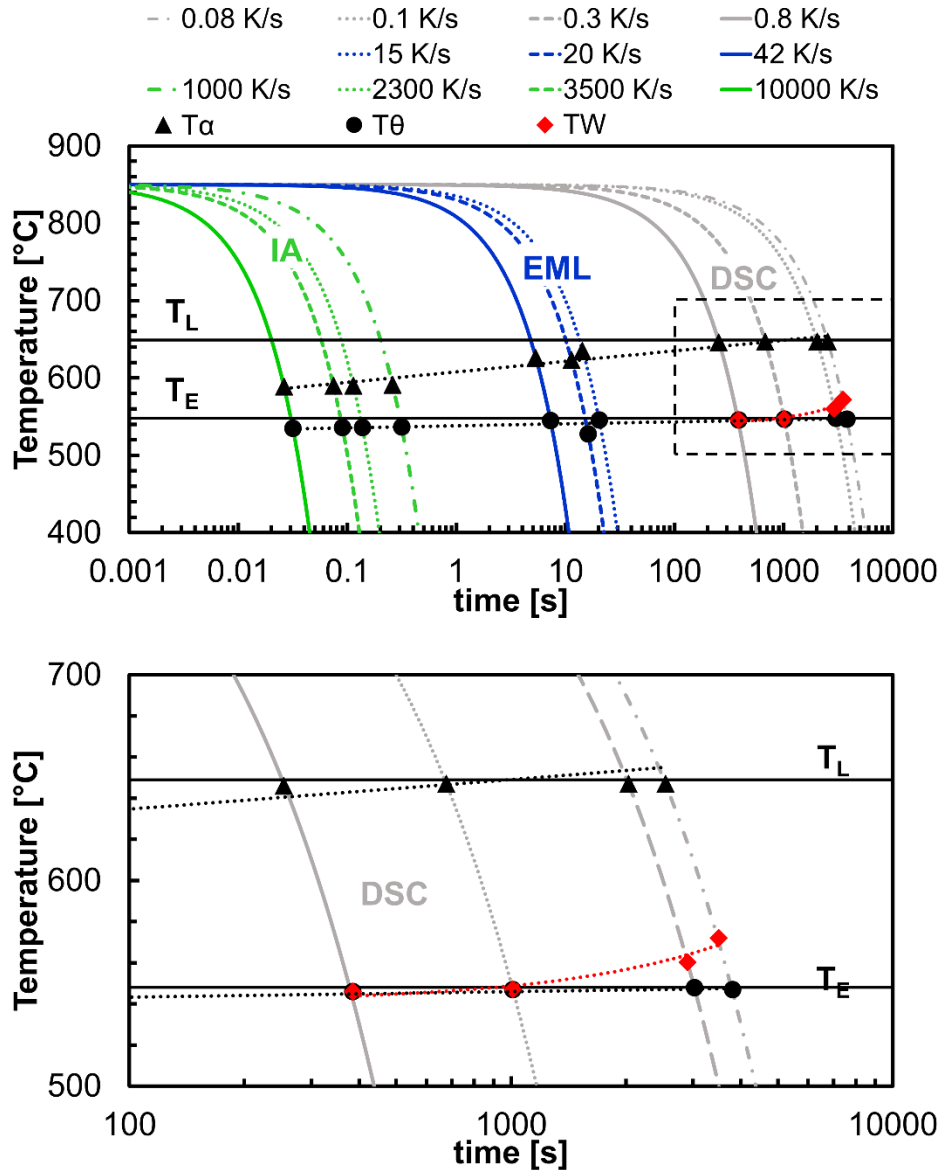
264 these results, it is observed that both primary phase and eutectic nucleation undercoolings
 265 increase as the cooling rate is increased. Also, to avoid the formation of the detrimental ternary
 266 W-phase, a cooling rate of the order of 1 K/s is necessary.

267 The use of the SCCT diagrams is not restricted to solidifying liquid droplets but should apply to
 268 any liquid of the Al-4.5wt%Cu-(0.4wt%Sc) composition solidifying in any given solidification
 269 process. Limitations to the use of this diagram will occur when there is significant segregation of
 270 Cu during solidification. However, in these instances, similar SCCT diagrams may be derived
 271 using droplet cooling rates for alloys with different Cu compositions, to trace the path of
 272 solidification of a given alloy in a particular process. This is the subject of further research.



273

274 **Figure 11:** Solidification Continuous Cooling Transformation curves of Al-4.5wt%Cu.



275

276 **Figure 12:** Top: Solidification Continuous Cooling Transformation curves of Al-4.5wt%Cu-

277 0.4wt%Sc. Bottom: Magnified view of the nucleation temperatures of the ternary W-phase.

278

279 Conclusions

280 Al-4.5wt% Cu with different level of Sc addition (0, 0.2 and 0.4wt%) were generated under low,
 281 medium and high cooling rate conditions respectively by DSC, EML and IA. No refining effect of
 282 Sc is found. Cell spacing variation with cooling rate for the investigated alloys is found to follow
 283 an empirical coarsening law of secondary dendrite arms spacing commonly found in literature. Sc
 284 addition is shown to reduce both the primary and eutectic undercoolings in all three types of

285 solidification experiments carried out. This in turns promotes the formation of lower speed
286 morphologies as evidenced by the decrease of droplets exhibiting finger bundles in IA samples.

287 Using solidification continuous cooling transformation maps, the solidification path of Al-
288 4.5wt%Cu and Al-4.5wt%Cu-0.4wt%Sc has been charted over a wide range of cooling rates. An
289 increase in cooling rate leads to an increase of the primary and eutectic undercoolings. During
290 DSC experiments at low cooling rates, scandium induces the precipitation of the W-phase, which
291 is detrimental to the mechanical properties of the alloy. At higher cooling rates in EML and IA, the
292 precipitation of the W-phase is suppressed. The SCCT diagram shows that a minimum cooling
293 rate of about 1 K/s is required to avoid the nucleation of the detrimental intermetallic, W-phase.

294

295 **Acknowledgements**

296 Financial support from the Natural Sciences and Engineering Research Council of Canada
297 (NSERC) and the Holistic Innovation in Additive Manufacturing (HI-AM) Network, as well as the
298 European Space Agency (ESA) within the frame of the NEQUISOL project is gratefully
299 acknowledged. The authors are grateful to the Canadian Nuclear Laboratories (CNL) and the
300 European Synchrotron Radiation Facility (ESRF) for beam time and expert support during the
301 measurement campaigns. The assistance of Daniel Auras with morphology analysis is
302 appreciated.

303

304 **References**

305

- 306 [1] J. R. Davis (ed.). ASM Specialty Handbook: Aluminum and Aluminum Alloys. ASM
307 International 1993.
- 308 [2] Haasen, P. Physical Metallurgy, 3rd ed.; Cambridge University Press: Cambridge, UK,
309 1996.
- 310 [3] Sims, Z.C., Rios, O.R., Weiss, D., Turchi, P.E.A., Perron, A., Lee, J.R.I., Li, T.T.,
311 Hammons, J.A., Bagge-Hansen, M., Willey, T.M., An, K., Chen, Y., King, A.H., McCall,
312 S.K. High performance aluminum-cerium alloys for high-temperature applications (2017)
313 Materials Horizons, 4 (6), pp. 1070-1078.
- 314 [4] Blake, N., Hopkins, M.A. Constitution and age hardening of Al-Sc alloys (1985) Journal
315 of Materials Science, 20 (8), pp. 2861-2867.

- 316 [5] Seidman, D.N., Marquis, E.A., Dunand, D.C. Precipitation strengthening at ambient and
317 elevated temperatures of heat-treatable Al(Sc) alloys (2002) *Acta Materialia*, 50 (16),
318 pp. 4021-4035.
- 319 [6] L.S. Toporova, D.G. Eskin, M.L. Kharakterova, T.B. Dobatkina *Advanced aluminum*
320 *alloys containing scandium*, Gordon & Breach, Amsterdam (1998).
- 321 [7] Bogno, A.-A., Valloton, J., Henein, H., Ivey, D.G., Locock, A.J., Gallerneault, M. Effects
322 of scandium on hypoeutectic aluminium copper microstructures under low solidification
323 rate conditions (2018) *Canadian Metallurgical Quarterly*, 57 (2), pp. 148-159.
- 324 [8] Røyset, J., Ryum, N. Scandium in aluminium alloys (2005) *International Materials*
325 *Reviews*, 50 (1), pp. 19-44.
- 326 [9] J. Royset, Scandium in Aluminium alloys overview: Physical Metallurgy, Properties and
327 applications, *Metall. Sci. and Technology*, 2007 25 (2) pp. 11-21.
- 328 [10] Kharakterova, H.L., Dobatkina, T.V. Polythermal sections of the Al-Cu-Sc system (1988)
329 *Russian metallurgy. Metally*, (6), pp. 175-178.
- 330 [11] M. L. Kharakterova, "Phase composition of Al-Cu-Sc alloys at 450 and 500°C" *Metally*,
331 No. 4, 191-194 (1991).
- 332 [12] Bo, H., Liu, L.B., Jin, Z.P. Thermodynamic analysis of Al-Sc, Cu-Sc and Al-Cu-Sc system
333 (2010) *Journal of Alloys and Compounds*, 490 (1-2), pp. 318-325.
- 334 [13] Riva, S., Yusenko, K.V., Lavery, N.P., Jarvis, D.J., Brown, S.G.R. The scandium effect
335 in multicomponent alloys (2016) *International Materials Reviews*, 61 (3), pp. 203-228.
- 336 [14] Andersson JO, Helander T, Höglund L, et al. Thermo-Calc and Dictra, computational
337 tools for materials science. *Calphad*. 2002;26:273–312
- 338 [15] Bogno, A.-A., Valloton, J., Henein, H., Gallerneault, M., Herlach, D. Effect of
339 hypoeutectic Sc additions to Al-4.5 wt% Cu under different cooling rates (2017) *Minerals,*
340 *Metals and Materials Series*, (9783319521312), pp. 355-363.
- 341 [16] H. Henein, "Single fluid atomization through the application of impulses to a melt,"
342 *Materials Science and Engineering*, vol. A326, pp. 92-100, 2002.
- 343 [17] J. Wiskel, H. Henein and E. Maire, "Solidification study of aluminum alloys using impulse
344 atomization: part i: heat transfer analysis of an atomized droplet," *Canadian Metallurgical*
345 *Quarterly*, vol. 41, no. 1, pp. 97-110, 2002.
- 346 [18] J. Wiskel, K. Navel, H. Henein and E. Maire, "Solidification study of aluminum alloys
347 using impulse atomization: part ii: effect of cooling rate on microstructure," *Canadian*
348 *Metallurgical Quarterly*, vol. 41, no. 2, pp. 193-204, 2002.

- 349 [19] Bogno, A.-A., Khatibi, P.D., Henein, H., Gandin, C.-A. Quantification of Primary Dendritic
350 and Secondary Eutectic Nucleation Undercoolings in Rapidly Solidified Hypo-Eutectic
351 Al-Cu Droplets (2016) Metallurgical and Materials Transactions A: Physical Metallurgy
352 and Materials Science, 47 (9), pp. 4606-4615.
- 353 [20] R. A. Young (ed.). The Rietveld Method. International Union of Crystallography. Oxford
354 University Press 1993.
- 355 [21] D. M. Herlach and D. M. Matson: Solidification of Containerless Undercooled Melts,
356 Wiley-VCH, Weinheim, 1st ed, 2012, pp. 9-16.
- 357 [22] Chen, J., Dahlborg, U., Bao, C.M., Calvo-Dahlborg, M., Henein, H. Microstructure
358 evolution of atomized Al-0.61 wt pct Fe and Al-1.90 wt pct Fe alloys (2011) Metallurgical
359 and Materials Transactions B: Process Metallurgy and Materials Processing Science,
360 42 (3), pp. 557-567.
- 361 [23] Bedel, M., Reinhart, G., Bogno, A.-A., Gandin, Ch.-A., Jacomet, S., Boller, E., Nguyen-
362 Thi, H., Henein, H. Characterization of dendrite morphologies in rapidly solidified Al-4.5
363 wt.%Cu droplets (2015) Acta Materialia, 89, pp. 234-246.
- 364 [24] Eskin, D., Du, Q., Ruvalcaba, D., Katgerman, L. Experimental study of structure
365 formation in binary Al-Cu alloys at different cooling rates (2005) Materials Science and
366 Engineering A, 405 (1-2), pp. 1-10.
- 367 [25] Mullis, A.M., Farrell, L., Cochrane, R.F., Adkins, N.J. Estimation of cooling rates during
368 close-coupled gas atomization using secondary dendrite arm spacing measurement
369 (2013) Metallurgical and Materials Transactions B: Process Metallurgy and Materials
370 Processing Science, 44 (4), pp. 992-999.
- 371 [26] J. A. Dantzig and M. Rappaz, Solidification, Lausanne: EPFL Press, 2009.
- 372